Orientation dependent elastic stress concentration at tips of slender objects translating in viscoelastic fluids

Chuanbin Li, Becca Thomases, and Robert D. Guy

Orientation dependent elastic stress concentration at tips of slender objects translating in viscoelastic fluids

Chuanbin Li

Department of Mathematics, The Pennsylvania State University, University Park, PA 16802

Becca Thomases and Robert D. Guy

Department of Mathematics, University of California Davis, Davis, CA 95616

(Dated: February 28, 2019)

Elastic stress concentration at tips of long slender objects moving in viscoelastic fluids has been observed in numerical simulations, but despite the prevalence of flagellated motion in complex fluids in many biological functions, the physics of stress accumulation near tips has not been analyzed. Here we theoretically investigate elastic stress development at tips of slender objects by computing the leading order viscoelastic correction to the equilibrium viscous flow around long cylinders, using the weak-coupling limit. In this limit nonlinearities in the fluid are retained allowing us to study the biologically relevant parameter regime of high Weissenberg number. We calculate a stretch rate from the viscous flow around cylinders to predict when large elastic stress develops at tips, find thresholds for large stress development depending on orientation, and calculate greater stress accumulation near tips of cylinders oriented parallel to motion over perpendicular.

I. INTRODUCTION

The interaction of slender objects such as cilia and flagella with surrounding viscoelastic fluid environments occurs in many important biological functions such as sperm swimming in mucus during fertilization and mucus clearance in the lungs. There has been much work devoted to understanding the effect of fluid elasticity in such systems including biological and physical experiments [1–4], asymptotic analysis for infinite-length swimmers [5–13], and numerical simulations of finite-length swimmers [14–19]. While flows around slender finite-length objects are essential to our understanding of the physics of micro-organism locomotion, our understanding of these flows in viscoelastic fluids is limited. Previous experimental and theoretical results have focused largely on sedimentation of slender particles in the limit of vanishing relaxation time, i.e. the low Weissenberg number limit [20–26].

Numerical simulations of flagellated swimmers in viscoelastic fluids have shown the concentration of polymer elastic stress at the tips of slender objects [14, 16, 18, 19], (see Fig. 1) but why the stress concentrates so strongly at tips, and the effect of these stresses on micro-organism locomotion is not understood. Unlike asymptotic theory [7–10, 12, 13] these simulations involve large amplitude motions of finite length objects, and these large elastic stresses that arise have a substantially different effect on swimming motion than predicted by asymptotic analysis [18]. Experiments can measure kinematic changes [1, 4], but not elastic stress, and thus the mechanisms of observed behavioral responses cannot be explained by experiments alone.
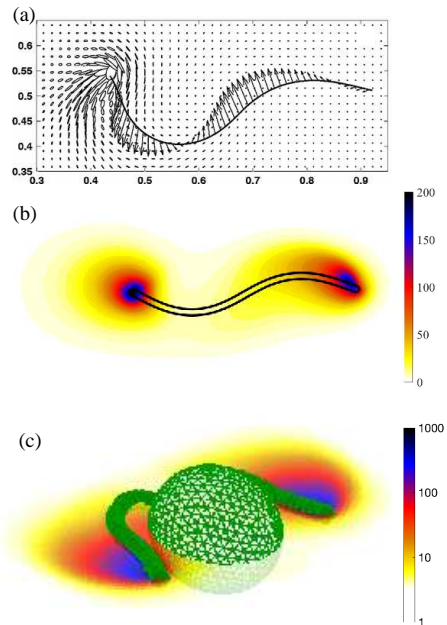
It was observed in simulations [19] that the con-

FIG. 1. (a) 2D flow around large amplitude, finite-length undulatory swimmer, ellipses show size and orientation of stress concentrated at tail (reproduced from [14]). (b) 2D flow around bending sheet, color field shows strain energy density concentrated at tips. (c) 3D flow around swimming bi-flagellated cell, color field in center plane shows strain energy density.

centrated tip stresses are stronger for a cylinder moving parallel to its axis compared to a cylinder moving perpendicular to its axis. This orientation dependence of elastic stress at tips is reversed from the orientation dependence of force on velocity in resistive

force theory and related viscous fluid theories [27–32] which form the basis of much of our intuition about micro-organism locomotion without inertia. Classical viscous theories do not include tip effects, but previous results in viscoelastic fluids [14, 16, 18, 19] suggest that the tip has a special role in the elastic stress development which has not been previously analyzed.

Previous work on the flow of viscoelastic fluids around slender objects has been done in the weakly nonlinear (or low Weissenberg number, Wi) regime [20–26], but the large stress concentration at tips of thin objects is a nonlinear effect and thus cannot be captured in a low Wi expansion. However, the highly nonlinear regime is challenging for numerical simulations [33], and this has limited the ability to probe dynamics in this regime. As another approach, one can consider the limit of low polymer concentration, decoupling the stress and velocity. This method has been used to study stress localization for high-Wi at extensional points and around objects [34–38].

The weak coupling expansion, a formal asymptotic approximation in the limit of low polymer concentration, retains viscoelastic nonlinearities at leading order [39]. This method has been successful in capturing high Wi effects for flow around a sphere in 3D [39], and in the study of the rheology of dilute suspensions in the low polymer concentration limit [40]. Similar stress localization in the wake of spheres has been observed experimentally [41, 42] and theoretical predictions of shear thickening for strongly elastic dilute suspensions were in agreement with experimental observations [43].

Here we use the weak coupling expansion to study the equilibrium flow around, and resultant force on, cylinders translating either perpendicular, or parallel to the direction of motion, in a 3D viscoelastic fluid. Using this analysis we explain the origin of the tip stresses, we predict a critical Weissenberg number for the flow transition based on viscous flow data, and we show how the tip stress accumulation depends on cylinder orientation.

II. MODEL EQUATIONS

We examine the viscoelastic fluid flow around a stationary finite-length cylinder of radius a with hemispherical caps driven by a fixed flow at infinity, $\mathbf{U}_\infty$. We use the Oldroyd-B model of a viscoelastic fluid at zero Reynolds number, which is attractive as a frame-invariant, nonlinear, continuum model of a viscoelastic fluid that can capture the dominant effects of fluid elasticity, e.g. storage of history of deformation on a characteristic time-scale. The di-

mensionless system of equations is given by

$$\Delta\mathbf{u} - \nabla p + \beta\nabla\cdot\mathbf{C} = 0, \tag{1}$$

$$\nabla\cdot\mathbf{u} = 0, \tag{2}$$

$$\mathcal{D}_t[\mathbf{u}]\mathbf{C} = \mathrm{Wi}^{-1}\mathbf{I} + \left(\nabla\mathbf{u}\mathbf{C} + \mathbf{C}\nabla\mathbf{u}^T\right) - \mathrm{Wi}^{-1}\mathbf{C}, \tag{3}$$

for $\mathbf{u}$ the fluid velocity, p the fluid pressure, and $\mathbf{C}$, the conformation tensor, a macroscopic average of the polymer orientation and stretching that is related to the polymer stress tensor by $\boldsymbol{\sigma}^p = \beta(\mathbf{C}-\mathbf{I})$. We use $\mathcal{D}_t[\mathbf{u}]$ to denote the material time derivative along the velocity field $\mathbf{u}$. The parameters, β, the non-dimensional polymer stiffness, and Wi, the Weissenberg number, or non-dimensional relaxation time, are defined by

$$\beta = \frac{Gr}{\mu U}, \quad \mathrm{Wi} = \frac{\lambda U}{r}, \tag{4}$$

for μ the fluid viscosity, λ the fluid relaxation time, G the polymer elastic modulus, and $U = |\mathbf{U}_\infty|$.

The force on a stationary cylinder in a background flow is proportional to the rate at which energy is dissipated by the fluid. To calculate the dissipation rate we integrate the dot product of $(\mathbf{u} - \mathbf{U}_\infty)$ and Eq. (1) over the fluid domain, Ω (exterior to the cylinder). After some manipulations and using the incompressibility constraint we obtain

$$\mathbf{U}_\infty\cdot\mathbf{F} = 2\int_\Omega D_{ij}D_{ij}\,dV + \beta\int_\Omega \frac{\partial u_i}{\partial x_j}C_{ij}\,dV, \tag{5}$$

where $D_{ij} = \frac{1}{2}\left(\frac{\partial u_i}{\partial x_j} + \frac{\partial u_j}{\partial x_i}\right)$ is the rate of strain tensor, $\mathbf{F} = \int_{\partial\Omega}(\boldsymbol{\sigma}^n + \beta\mathbf{C})\cdot\mathbf{n}\,dS$ is the force on the cylinder, and $\boldsymbol{\sigma}^n = 2\mathbf{D} - p\mathbf{I}$ is the Newtonian stress tensor. Thus for a constant velocity at infinity the force on the cylinder is proportional to the sum of the viscous dissipation rate and the rate at which energy is transferred to the polymers.

The polymer strain energy is $\mathcal{E} = \int_\Omega \mathrm{Tr}(\mathbf{C}-\mathbf{I})\,dV$ [44], and an equation for the strain energy is obtained by taking the trace of Eq. (3) and integrating over the fluid domain,

$$\frac{d}{dt}\mathcal{E} = 2\int_\Omega \frac{\partial u_i}{\partial x_j}C_{ij}\,dV - \mathrm{Wi}^{-1}\mathcal{E}. \tag{6}$$

Changes in the polymer energy come from transfer of energy between the fluid and the polymer and energy lost to polymer relaxation. Therefore at steady state the rate of energy loss to the fluid is proportional to the polymer energy. By combining Eq. (5) with Eq. (6) one finds that at steady state the force on the cylinder is

$$\mathbf{U}_\infty\cdot\mathbf{F} = 2\int_\Omega D_{ij}D_{ij}\,dV + \frac{\beta}{2\mathrm{Wi}}\mathcal{E}. \tag{7}$$

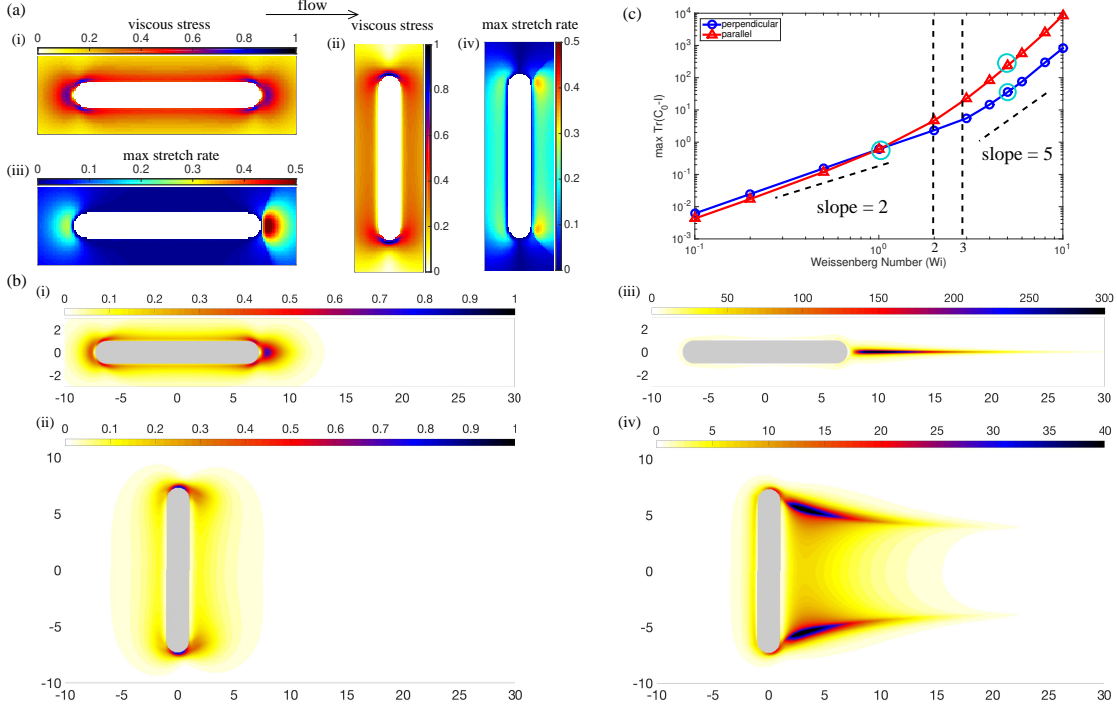Hence the strain energy $\mathcal{E}$ quantifies the force on the cylinder due to viscoelasticity.

FIG. 2. (a) Norm of viscous stress in the center plane for cylinders oriented (i) parallel $(\max\|2\mathbf{D}_0^{\parallel}\| \approx 0.78)$ and (ii) perpendicular $(\max\|2\mathbf{D}_0^{\perp}\| \approx 0.95)$ to flow; stretch rates of viscous flow for cylinders oriented (iii) parallel $(\max\nu^{\parallel} \approx 0.5)$ and (iv) perpendicular $(\max\nu^{\perp} \approx 0.34)$ to flow. Flow goes from left to right. (b) $\mathrm{Tr}(\mathbf{C}_0 - \mathbf{I})$ in the center plane for cylinders with (i)-(ii) Wi = 1 and (iii)-(iv) Wi = 5 (note the difference in scale). (c) Maximum of $\mathrm{Tr}(\mathbf{C}_0 - \mathbf{I})$ as a function of Wi for the two orientations, in log scales. Dotted lines show the two critical Weissenberg numbers Wi ≈ 2, and Wi ≈ 3, cyan circles indicate Wi values pictured in (b).

III. WEAK-COUPLING EXPANSION

Previous theoretical results on the polymeric contribution to a translating cylinder have used a second-order fluid expansion in the weakly nonlinear regime [26, 45–48], where the nonlinearities associated with viscoelasticity are lost at leading order. We are interested in the regime of large amplitude motions where large stress accumulates in the fluid, so we consider the *weakly coupled*, or small β, regime where the nonlinearities enter at leading order but the coupling between the polymer and fluid is higher order. The weak coupling expansion was introduced for flow around a sphere in [39], and is similar to analysis of viscoelastic fluids using fixed velocity fields in the high Wi regime [49, 50]. Analysis of viscoelastic fluids with fixed velocity fields have predicted transitions in behavior for high Wi at steady extensional points [34–38] and qualitatively similar transitions are also found in simulations where the velocity and the stress are fully coupled [38].

We expand the solutions in β, $\mathbf{u} \sim \mathbf{u}_0 + \beta\mathbf{u}_1$, $p \sim p_0 + \beta p_1$, and $\mathbf{C} \sim \mathbf{C}_0 + \beta\mathbf{C}_1$. At leading order

Eqs. (1)–(2) decouple from Eq. (3), and $\mathbf{u}_0$ is the solution for the viscous flow around the cylinder. The conformation tensor satisfies

$$\mathcal{D}_t[\mathbf{u}_0]\mathbf{C}_0 = \mathrm{Wi}^{-1}\mathbf{I} + \mathcal{S}[\mathbf{u}_0]\mathbf{C}_0 - \mathrm{Wi}^{-1}\mathbf{C}_0, \quad (8)$$

where $\mathcal{S}[\mathbf{u}_0]\mathbf{C}_0 \equiv \left(\nabla\mathbf{u}_0\mathbf{C}_0 + \mathbf{C}_0\nabla\mathbf{u}_0^T\right)$. On a given streamline Eq. 8 is an ODE involving a source term, $\mathrm{Wi}^{-1}\mathbf{I}$, a stretching term, $\mathcal{S}[\mathbf{u}_0]$, and a relaxation term, $\mathrm{Wi}^{-1}\mathbf{C}_0$.

IV. TIP STRESS DEVELOPMENT

We prescribe a unit flow in the x−direction, $\mathbf{U}_\infty = \mathbf{e}_x$, in the domain exterior to a cylinder that is oriented either parallel or perpendicular to the direction of flow, with no-slip boundary conditions on the cylinder walls. The circular cylinder has length 4π, radius $a = 1$, and is capped at both ends with hemispheres. We solve the Stokes equations for $\mathbf{u}_0$ using a boundary integral method based on a regularized Green's function from the method of regularized Stokeslets [51–53]. We generate streamlines

of the Newtonian flow $\mathbf{u}_0$ and evolve Eq. (8) along those streamlines. See Supplemental Material for more details [54].

In Fig. (2) (a) we plot the Frobenius norm (defined $\|\mathbf{A}\| \equiv \sqrt{A_{ij}A_{ij}}$) of the leading order viscous stress tensor $2\mathbf{D}_0$ in the center plane for cylinders oriented (i) parallel and (ii) perpendicular to the flow. Note that the viscous stress near the middle of the cylinders is 2 or 3 times smaller than that at the tips. In Fig. 2 (b) we show color fields of the leading order polymer strain energy density $\mathrm{Tr}(\mathbf{C}_0 - \mathbf{I})$, for two different Weissenberg numbers (i)-(ii) $\mathrm{Wi} = 1$ and (iii)-(iv) $\mathrm{Wi} = 5$. For $\mathrm{Wi} = 1$ the elastic stress is concentrated at the tips like the viscous stress, and on the same scale as the viscous stress. For $\mathrm{Wi} = 5$ however, the elastic stress at the tips is more than 100 times larger than for $\mathrm{Wi} = 1$, and concentrated in the wake. This nonlinear response has been seen before in analysis of flow around a circle in 2D [55–57] and around a sphere in 3D [39]. However, in Fig. 2 (b) (iii)-(iv) we also see that the stress in the wake of the cylinder that is oriented parallel to the direction of the flow is about 10 times larger than that for the cylinder oriented perpendicular to the direction of flow. We examine the Newtonian flow that drives the stress growth to understand what sets the transition in Wi, and how the cylinder orientation impacts stress growth so dramatically for large Wi.

At a fixed point in the flow, the real parts of the eigenvalues of the operator $\mathcal{S}[\mathbf{u}_0]$, defined in Eq. (8), set the growth (or decay) rates of $\mathbf{C}_0$ due to stretching (or compression). The solution to the eigenvalue problem $\mathcal{S}[\mathbf{u}]\mathbf{C} = \nu\mathbf{C}$ is $\mathbf{C} = \mathbf{v}_i\mathbf{v}_j^T$, $\nu_{ij} = \mu_i + \mu_j$, where μ_i is an eigenvalue of $\nabla\mathbf{u}$ with corresponding eigenvector $\mathbf{v}_i$. We define the max stretch rate ν at a point as

$$\nu = 2\max(\mathrm{Re}(\Lambda(\nabla\mathbf{u}_0))), \tag{9}$$

where $\Lambda(A)$ is the set of eigenvalues of the matrix A. In regions of the flow where $\nu - \mathrm{Wi}^{-1} > 0$, or $\nu\mathrm{Wi} > 1$, stretching outpaces relaxation, and while fluid particles remain in these stretching regions they experience unbounded stress growth.

In Fig. 2 (a) we plot ν in the center plane for the cylinder oriented parallel (iii) and the cylinder oriented perpendicular (iv). The maximum stretch rate for both cylinders occurs in the wake of the cylinder, i.e. the max stretch rate contains information about flow directionality that is missing from Fig. (2) (a) (i)-(ii). We see that the cylinder oriented parallel to motion has $\max(\nu^\parallel) \approx 0.5$, thus $\mathrm{Wi}^\parallel \approx 2$ is a threshold for stretching outpacing relaxation in regions of this flow. The maximum for the perpendicularly oriented cylinder is smaller, $\max(\nu^\perp) \approx 0.34$, corresponding to a threshold $\mathrm{Wi}^\perp \approx 3$ for large stress

growth. For the perpendicularly oriented cylinder, the flow in the regions of high viscous stress near the tip is locally a shear flow, whereas, the local flow is extensional (which is known to lead to more rapid elastic stress growth [58]) near the tips of the cylinder oriented parallel. The difference in flow type is reflected in the max stretch rate which is largest near the trailing tip of the cylinder oriented parallel to motion where the viscous stress is largest. For the perpendicularly oriented cylinder, the strongest extension is behind the cylinder where the viscous stresses are weaker.

In Fig. 2 (c) we plot $\max\mathrm{Tr}(\mathbf{C}_0 - \mathbf{I})$ for $\mathrm{Wi} \le 10$. For both orientations, the maximum of $\mathrm{Tr}(\mathbf{C}_0 - \mathbf{I})$ scales like Wi^2 below $\mathrm{Wi} \approx 2$, and scales like Wi^5 above $\mathrm{Wi} \approx 3$. The cylinder oriented parallel to motion has a larger max stretch rate and thus it enters the regime of large stress growth for lower Wi than the perpendicularly oriented cylinder, leading to larger stress for a fixed Wi beyond the threshold $\mathrm{Wi}^\parallel \approx 2$. Recall that the contribution to the force from the polymeric stress scales like $\frac{\beta}{2\mathrm{Wi}}\mathcal{E}$ and thus for low Wi there is a $\mathcal{O}(\mathrm{Wi})$ contribution to the force whereas for high Wi the contribution is $\mathcal{O}(\mathrm{Wi}^4)$. Theoretical results have predicted similar scalings for related problems [39, 49, 50].

V. VISCOELASTIC CORRECTION TO FORCE

We expand the force on a cylinder to first order in β as

$$\mathbf{F} \sim \int_{\partial\Omega} \boldsymbol{\sigma}_0^n \cdot \mathbf{n} + \beta\left(\boldsymbol{\sigma}_1^n + \mathbf{C}_0\right) \cdot \mathbf{n}\ dS \equiv \mathbf{F}_0 + \beta\mathbf{F}_1. \tag{10}$$

We avoid computing $\mathbf{u}_1$, the first-order correction to the velocity, by using reciprocal relations [26, 45–48], as has been done before in many calculations of non-Newtonian corrections at low Reynolds number. In addition, because the flow and force are parallel for these orientations, we obtain the magnitude of $\mathbf{F}_1$ as

$$F_1 = \mathrm{Wi}^{-1}\int_\Omega \mathrm{Tr}(\mathbf{C}_0 - \mathbf{I})\ dV. \tag{11}$$

Details of our calculation are provided in Supplemental Material [54]. Thus the viscoelastic correction to the force is proportional to the integral of the trace of the leading order polymer stress tensor over the fluid domain.

In Fig. 3 (a) we plot the viscoelastic force correction, F_1, normalized by $F_0^\perp = 65$ (note $F_0^\parallel = 48$) for $\mathrm{Wi} \le 10$ for each cylinder orientation. We see that in the expansion the $\mathcal{O}(\beta)$ force correction is up to 25
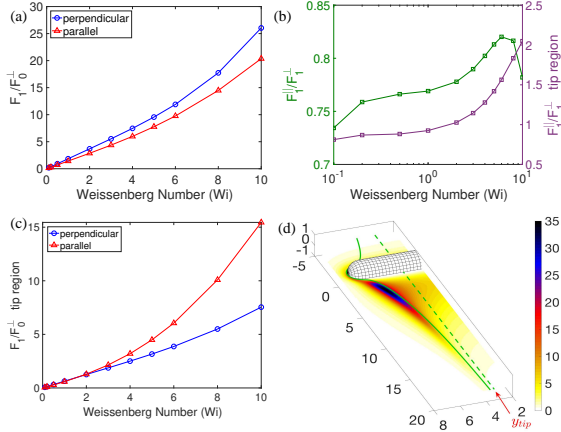
FIG. 3. (a) $F_1/F_0^{\perp}$ (perpendicular and parallel) (b) parallel to perpendicular ratio of F_1 : whole domain (left axes), tip region (right axes) (c) F_1 restricted to tip (perpendicular and parallel) (d) Diagram illustrating definition of y_{tip}.

times the viscous force for large Wi. The perpendicular force correction is larger than the parallel force correction, however Fig. 3 (b) shows $F_1^{\parallel}/F_1^{\perp}$ (left hand axes) and beyond Wi ≈ 2 (the parallel stress growth threshold) $F_1^{\parallel}$ increases more than $F_1^{\perp}$, and this continues until about Wi ≈ 6 where the ratio starts to decrease again. Since we are interested in the "tip effect", we calculate the contribution to the force from a single tip.

We define this tip force by restricting the integration domain in Eq. (11) to a subdomain exterior to the cylinder that contains only one tip. In Fig. 3 (d) we show the tip of the perpendicular cylinder with the strain energy density for Wi $= 5$. We consider a streamline that approaches very close to the tip in the center plane and we evolve the streamline until it levels off for large x, and we define the value it approaches, $y_{\text{tip}} = 3.41$, as shown in Fig. 3 (d). With this we define

$$F_1^{\text{tip}} = \text{Wi}^{-1} \int_{\Omega \setminus \{y < y_{\text{tip}}\}} \text{Tr}(\mathbf{C}_0 - \mathbf{I}) \, dV. \quad (12)$$

In Fig. 3 (c) we plot $F_1^{\text{tip}}/F_0^{\perp}$ for Wi ≤ 10 for each cylinder orientation, and the ratio of tip force corrections in Fig. 3(b) (right hand axes). Beyond the threshold Wi$^{\parallel} \approx 2$, the parallel force correction at the tip is larger than the perpendicular force correction, and the parallel force correction is double the perpendicular force correction from the tip at high Wi.

VI. DISCUSSION

Using the viscous flow field around cylinders we predict a critical Wi beyond which a large stress "tip effect" occurs, and we find that the critical Wi is orientation dependent. There are larger elastic stresses in the wake of cylinders oriented parallel to the direction of motion compared to cylinders oriented perpendicular to the flow. The flow type (shear or extensional) is orientation dependent and is reflected in the larger max stretch rate for the cylinder oriented parallel. The max stretch rate is defined from the eigenvalues of the operator $\mathcal{S}$ in Eq. (8), and this operator appears in all differential models of viscoelasticity, including models which incorporate additional non-Newtonian effects such as shear-thinning. Hence we conjecture that the transitions we have identified are not specific to the Oldroyd-B model, although quantitative values of stress accumulation beyond the transitions will depend on the model.

We explored other tip shapes and found that varying curvature at the tip did not effect the qualitative results; the max stretch rate was always largest near the tip, and greater for cylinders oriented parallel to the motion. The analysis given used the rod thickness to define the characteristic length scale and hence thinner rods will exhibit large stress growth at a lower relaxation time. Although the tip effect is independent of the length, the relative contribution to the total force from the tip depends on the length, and hence, quantifying the role of the tip effect on locomotion requires more investigation. Nevertheless, based on past numerical simulations of flagellated swimmers, it is clear that this tip effect is significant.

In [19] we observed elastic stress accumulation at flagellar tips in a simulation of a bi-flagellated alga cell swimming using experimentally measured kinematics. The stress accumulation was greater on the return stroke when the flagellar tips were oriented parallel to the direction of motion than when oriented perpendicular to the motion. The steady-state analysis of the tip effect presented here helps explain the physics behind these observations made in [19], but generally details of stroke kinematics, including time-dependence, will effect how stresses develop around flagellated swimmers. We are able to make predictions about critical Weissenberg numbers for steady flows by looking at the max stretch rates, but this tool could be useful for other gaits and even in experimental settings where flow fields are obtainable but location and concentration of stress are not measurable.

[1] XN Shen and Paulo E Arratia, "Undulatory swimming in viscoelastic fluids," Physical review letters **106**, 208101 (2011).

[2] Bin Liu, Thomas R Powers, and Kenneth S Breuer, "Force-free swimming of a model helical flagellum in viscoelastic fluids," Proceedings of the National Academy of Sciences **108**, 19516–19520 (2011).

[3] Julian Espinosa-Garcia, Eric Lauga, and Roberto Zenit, "Fluid elasticity increases the locomotion of flexible swimmers," Physics of Fluids (1994-present) **25**, 031701 (2013).

[4] Boyang Qin, Arvind Gopinath, Jing Yang, Jerry P Gollub, and Paulo E Arratia, "Flagellar kinematics and swimming of algal cells in viscoelastic fluids," Scientific reports **5**, 9190 (2015).

[5] T. K. Chaudhury, "On swimming in a visco-elastic liquid," Journal of Fluid Mechanics **95**, 189-197 (1979).

[6] Glenn R Fulford, David F Katz, and Robert L Powell, "Swimming of spermatozoa in a linear viscoelastic fluid," Biorheology **35**, 295–309 (1998).

[7] Henry C Fu, Thomas R Powers, and Charles W Wolgemuth, "Theory of swimming filaments in viscoelastic media," Physical review letters **99**, 258101 (2007).

[8] Henry C Fu, Charles W Wolgemuth, and Thomas R Powers, "Beating patterns of filaments in viscoelastic fluids," Physical Review E **78**, 041913 (2008).

[9] Eric Lauga, "Propulsion in a viscoelastic fluid," Phys. Fluids **19**, 83104 (2007).

[10] Henry C Fu, Charles W Wolgemuth, and Thomas R Powers, "Swimming speeds of filaments in nonlinearly viscoelastic fluids," Physics of Fluids (1994-present) **21**, 033102 (2009).

[11] Moumita Dasgupta, Bin Liu, Henry C Fu, Michael Berhanu, Kenneth S Breuer, Thomas R Powers, and Arshad Kudrolli, "Speed of a swimming sheet in Newtonian and viscoelastic fluids," Physical Review E **87**, 13015 (2013).

[12] Emily E Riley and Eric Lauga, "Enhanced active swimming in viscoelastic fluids," EPL (Europhysics Letters) **108**, 34003 (2014).

[13] Gwynn J Elfring and Gaurav Goyal, "The effect of gait on swimming in viscoelastic fluids," Journal of Non-Newtonian Fluid Mechanics **234**, 8–14 (2016).

[14] Joseph Teran, Lisa Fauci, and Michael Shelley, "Viscoelastic fluid response can increase the speed and efficiency of a free swimmer," Physical review letters **104**, 038101 (2010).

[15] Saverio E Spagnolie, Bin Liu, and Thomas R Powers, "Locomotion of helical bodies in viscoelastic fluids: enhanced swimming at large helical amplitudes," Physical review letters **111**, 068101 (2013).

[16] Becca Thomases and Robert D Guy, "Mechanisms of elastic enhancement and hindrance for finite-length undulatory swimmers in viscoelastic fluids," Physical review letters **113**, 098102 (2014).

[17] Daniel Salazar, Alexandre M. Roma, and Hector D. Ceniceros, "Numerical study of an inextensible, finite swimmer in Stokesian viscoelastic flow," Physics of Fluids **28**, 063101 (2016).

[18] Becca Thomases and Robert D Guy, "The role of body flexibility in stroke enhancements for finite-length undulatory swimmers in viscoelastic fluids," Journal of Fluid Mechanics **825**, 109–132 (2017).

[19] Chuanbin Li, Boyang Qin, Arvind Gopinath, Paulo E Arratia, Becca Thomases, and Robert D Guy, "Flagellar swimming in viscoelastic fluids: role of fluid elastic stress revealed by simulations based on experimental data," Journal of The Royal Society Interface **14**, 20170289 (2017).

[20] LG Leal, "The slow motion of slender rod-like particles in a second-order fluid," Journal of Fluid Mechanics **69**, 305–337 (1975).

[21] Sangtae Kim, "The motion of ellipsoids in a second order fluid," Journal of non-newtonian fluid mechanics **21**, 255–269 (1986).

[22] K Chiba, Ki-Won Song, and A Horikawa, "Motion of a slender body in quiescent polymer solutions," Rheologica acta **25**, 380–388 (1986).

[23] DD Joseph, "Flow induced microstructure in newtonian and visoelastic fluids," UMSI research report/University of Minnesota (Minneapolis, Mn). Supercomputer institute **99**, 97 (1996).

[24] PY Huang, Howard H Hu, and Daniel D Joseph, "Direct simulation of the sedimentation of elliptic particles in oldroyd-b fluids," Journal of Fluid Mechanics **362**, 297–326 (1998).

[25] Giovanni P Galdi, "Slow steady fall of rigid bodies in a second-order fluid," Journal of non-newtonian fluid mechanics **90**, 81–89 (2000).

[26] Vivekanand Dabade, Navaneeth K Marath, and Ganesh Subramanian, "Effects of inertia and viscoelasticity on sedimenting anisotropic particles," Journal of Fluid Mechanics **778**, 133–188 (2015).

[27] GJ Hancock, "The self-propulsion of microscopic organisms through liquids," Proceedings of the Royal Society of London A: Mathematical, Physical and Engineering Sciences **217**, 96–121 (1953).

[28] James Gray and GJ Hancock, "The propulsion of sea-urchin spermatozoa," Journal of Experimental Biology **32**, 802–814 (1955).

[29] Joseph B Keller and Sol I Rubinow, "Slender-body theory for slow viscous flow," Journal of Fluid Mechanics **75**, 705–714 (1976).

[30] James Lighthill, "Flagellar hydrodynamics," SIAM

review **18**, 161–230 (1976).

[31] RE Johnson and CJ Brokaw, "Flagellar hydrodynamics. a comparison between resistive-force theory and slender-body theory," Biophysical journal **25**, 113–127 (1979).

[32] Robert E Johnson, "An improved slender-body theory for Stokes flow," Journal of Fluid Mechanics **99**, 411–431 (1980).

[33] Robert G Owens and Timothy N Phillips, *Computational rheology* (World Scientific, 2002).

[34] JM Rallison and EJ Hinch, "Do we understand the physics in the constitutive equation?" Journal of Non-Newtonian Fluid Mechanics **29**, 37–55 (1988).

[35] OG Harlen, "High-deborah-number flow of a dilute polymer solution past a sphere falling along the axis of a cylindrical tube," Journal of Non-Newtonian Fluid Mechanics **37**, 157–173 (1990).

[36] OG Harlen, JM Rallison, and MD Chilcott, "High-deborah-number flows of dilute polymer solutions," Journal of Non-Newtonian Fluid Mechanics **34**, 319–349 (1990).

[37] Michael Renardy, "A comment on smoothness of viscoelastic stresses," Journal of non-newtonian fluid mechanics **138**, 204–205 (2006).

[38] Becca Thomases and Michael Shelley, "Emergence of singular structures in Oldroyd-B fluids," Physics of fluids **19**, 103103 (2007).

[39] Matthew NJ Moore and Michael J Shelley, "A weak-coupling expansion for viscoelastic fluids applied to dynamic settling of a body," Journal of Non-Newtonian Fluid Mechanics **183**, 25–36 (2012).

[40] Donald L Koch, Eric F Lee, and Ibrahim Mustafa, "Stress in a dilute suspension of spheres in a dilute polymer solution subject to simple shear flow at finite deborah numbers," Physical Review Fluids **1**, 013301 (2016).

[41] A Acharya, RA Mashelkar, and J Ulbrecht, "Flow of inelastic and viscoelastic fluids past a sphere," Rheologica Acta **15**, 454–470 (1976).

[42] Mark T Arigo and Gareth H McKinley, "An experimental investigation of negative wakes behind spheres settling in a shear-thinning viscoelastic fluid," Rheologica Acta **37**, 307–327 (1998).

[43] Rossella Scirocco, Jan Vermant, and Jan Mewis, "Shear thickening in filled boger fluids," Journal of rheology **49**, 551–567 (2005).

[44] Robert Byron Bird, Robert Calvin Armstrong, Ole Hassager, and Charles F Curtiss, *Dynamics of polymeric liquids*, Vol. 1 (Wiley New York, 1977).

[45] L Gary Leal, "The motion of small particles in non-newtonian fluids," Journal of Non-Newtonian Fluid Mechanics **5**, 33–78 (1979).

[46] John Happel and Howard Brenner, *Low Reynolds number hydrodynamics: with special applications to particulate media*, Vol. 1 (Springer Science & Business Media, 2012).

[47] Howard A Stone and Aravinthan DT Samuel, "Propulsion of microorganisms by surface distortions," Physical review letters **77**, 4102 (1996).

[48] Gwynn J Elfring, "A note on the reciprocal theorem for the swimming of simple bodies," Physics of Fluids **27**, 023101 (2015).

[49] Michael Renardy, "Asymptotic structure of the stress field in flow past a cylinder at high weissenberg number," Journal of non-newtonian fluid mechanics **90**, 13–23 (2000).

[50] P Wapperom and M Renardy, "Numerical prediction of the boundary layers in the flow around a cylinder using a fixed velocity field," Journal of non-newtonian fluid mechanics **125**, 35–48 (2005).

[51] Ricardo Cortez, "The method of regularized Stokeslets," SIAM Journal on Scientific Computing **23**, 1204–1225 (2001).

[52] Ricardo Cortez, Lisa Fauci, and Alexei Medovikov, "The method of regularized Stokeslets in three dimensions: analysis, validation, and application to helical swimming," Physics of Fluids **17**, 031504 (2005).

[53] C. Pozrikidis, *Boundary Integral and Singularity Methods for Linearized Viscous Flow* (Cambridge University Press, Cambridge, 1992).

[54] See Supplemental Material at [URL will be inserted by publisher] for details of the numerical method and validation, as well as a derivation of the force equation using reciprocal relations.

[55] Howard H Hu and Daniel D Joseph, "Numerical simulation of viscoelastic flow past a cylinder," Journal of Non-Newtonian Fluid Mechanics **37**, 347–377 (1990).

[56] Gareth H McKinley, Robert C Armstrong, and Robert Brown, "The wake instability in viscoelastic flow past confined circular cylinders," Phil. Trans. R. Soc. Lond. A **344**, 265–304 (1993).

[57] MA Alves, FT Pinho, and PJ Oliveira, "The flow of viscoelastic fluids past a cylinder: finite-volume high-resolution methods," Journal of Non-Newtonian Fluid Mechanics **97**, 207–232 (2001).

[58] Ronald G Larson, "The structure and rheology of complex fluids (topics in chemical engineering)," Oxford University Press, New York, Oxford **86**, 108 (1999).